Design and fabrication of the diffractive phase element that synthesizes three-color pseudo-nondiffracting beams

Jyh-Rou Sze
Mao-Hong Lu, MEMBER SPIE
National Chiao-Tung University
Institute of Electro-Optical Engineering
1001 Ta-Hsueh Road, Hsin-Chu 300
Taiwan, Republic of China (ROC).
E-mail: sze.eo88g@nctu.edu.tw

Abstract. The experimental implementation of the diffractive phase element (DPE) that synthesizes three-color psudo-nondiffracting beams (PNDBs) is described. This DPE is designed with the amplitude-phase retrieval method and fabricated by using optical contact lithography and reactive-ion etching (RIE). Measurements demonstrate that the fabricated DPE has the desired function, i.e., it forms a six-segment PNDB over a finite axial region and is monochromatic in each segment. © *2002 Society of Photo-Optical Instrumentation Engineers.* [DOI: 10.1117/1.1517287]

Subject terms: pseudo-nondiffracting beams; amplitude-phase retrieval method.

Paper 010123 received Apr. 4, 2001; revised manuscript received Mar. 18, 2002; accepted for publication May 7, 2002.

1 Introduction

Much recent effort has been devoted to design diffractive phase elements[1,2] (DPEs) because they can flexibly control a wavefront to perform diverse functions. Recently, the design and fabrication of the DPEs that can achieve various axial-illuminance modulations along the optical axis have been reported.[2–12]

DPEs that can produce nearly nondiffracting beams have also been suggested in the literature. The nondiffracting beam with field amplitude described by a zero-order Bessel function of the first kind was introduced[13] in 1987, and it has attracted great interest from researchers because of its possible applications in optical alignment, surveying, industrial inspection, and optical interconnection. Recently the concept of a pseudo-nondiffracting beam[14–19] (PNDB), characterized by an almost constant axial illuminance distribution over a finite axial region and a beamlike shape in the transverse dimension, has also been proposed. A PNDB must have a field amplitude near to the transverse Bessel beam distribution. A PNDB possesses unique properties, such as a uniform axial illuminance, a narrow lateral distribution, and a long propagation distance along the optical axis.

Recently Liu et al. employed the conjugate-gradient method to design DPEs that implement the monochromatic single-segment beam and multiple-segment beams,[17] and carried out the experimental implementations for a single-segment beam and double-segment beams.[18] With the same method, they also designed the DPEs that synthesize two-color four-segment beams.[19]

In this paper, we design three-color six-segment PNDBs in a multiple chromatic illuminating system, and show the simulation and the measurements for a DPE designed with the amplitude-phase retrieval method. As is well known, the amplitude-phase retrieval method has already been used in treating phase-retrieval problems, and later, its modified version has been applied to the design of DPE in the Fourier transform system.[20–22] We now apply this method to design DPEs in the Fresnel transform system for the case of multiple output planes. In Sec. 2 we introduce an error function for guiding the design of DPEs and appraising their performance. The relevant formulas used in the design are also described in Sec. 2. Section 3 describes the simulation and experimental results for the designed DPE. In this section, the transverse illuminance distributions of the beam in the segments are calculated and compared with those of the Bessel beam.

2 Theory of Amplitude-Phase Retrieval

We consider a rotationally symmetric optical system (see Fig. 1) illuminated by a beam with three wavelengths at $\lambda_1=0.6328\ \mu$m, $\lambda_2=0.5145\ \mu$m, and $\lambda_3=0.488\ \mu$m. A DPE is placed at the input plane P_1 of the system. The wave function at wavelength λ_α on the input plane can be written as

$$U_{1,\alpha}=U_1(r_1,\lambda_\alpha)=\rho_1(r_1,\lambda_\alpha)\exp[i\phi_1(r_1,\lambda_\alpha)]. \tag{1a}$$

The incident light at wavelength λ_α passes through the DPE and then propagates in free space. The corresponding wave function at the β'th output plane $P_{2,\alpha\beta}$, which is chosen along the optical axis of the system, can be given by

$$U_{2,\alpha\beta}=U_2(r_2,\lambda_\alpha,z_\beta)$$
$$=\rho_2(r_2,\lambda_\alpha,z_\beta)\exp\,[i\phi_2(r_2,\lambda_\alpha,z_\beta)]. \tag{1b}$$

In a Fresnel approximation, the field distribution on the output plane can be calculated by

Downloaded From: http://opticalengineering.spiedigitallibrary.org/ on 04/27/2014 Terms of Use: http://spiedl.org/terms

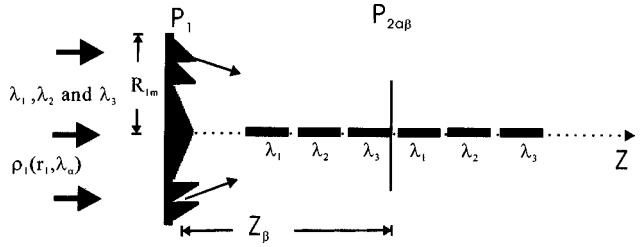

Fig. 1 Schematic of a diffractive optical system for producing PNDBs.

$$U_2(r_2,\lambda_\alpha,z_\beta)=\int G(r_1,r_2,\lambda_\alpha,z_\beta)U_1(r_1,\lambda_\alpha)\mathrm{d}r_1$$
$$=\frac{2\pi}{i\lambda_\alpha z_\beta}\exp(i2\pi z_\beta/\lambda_\alpha)\exp(i\pi r_2^2/\lambda_\alpha z_\beta)$$
$$\times\int_0^{R_{1m}}\rho_1(r_1,\lambda_\alpha)$$
$$\times\exp\left\{i\frac{2\pi}{\lambda_\alpha}[(n_\alpha-1)h(r_1)]\right\}J_0\left(\frac{2\pi r_1 r_2}{\lambda_\alpha z_\beta}\right)$$
$$\times\exp(i\pi r_1^2/\lambda_\alpha z_\beta)r_1\mathrm{d}r_1, \quad (2)$$

$$G(r_1,r_2,\lambda_\alpha,z_\beta)=\frac{2\pi}{i\lambda_\alpha z_\beta}\exp(i2\pi z_\beta/\lambda_\alpha)$$
$$\times\exp[i\pi(r_1^2+r_2^2)/\lambda_\alpha z_\beta]J_0\left(\frac{2\pi r_1 r_2}{\lambda_\alpha z_\beta}\right).$$

Here $J_0(2\pi r_1 r_2/\lambda_\alpha z_\beta)$ is the zeroth-order Bessel function of the first kind, the coordinate system is chosen such that the z axis is along the optical axis of the system, and r_1 and r_2 are the radial coordinates on the input and output plane, respectively; R_{1m} is the half diameter of the DPE; n_α is the refraction index of quartz substrate at wavelength λ_α; and $h(r_1)$ represents the surface-relief depth at the r_1 coordinate of the DPE. Equation (2) can be rewritten in a compact form as

$$U_2(r_2,\lambda_\alpha,z_\beta)=\hat{G}(r_1,r_2,\lambda_\alpha,z_\beta)U_1(r_1,\lambda_\alpha), \quad (3)$$

where $\hat{G}$ represents an integral. For a system with low loss and that satisfies the paraxial approximation, $\hat{G}$ is an unitary operator, i.e., $\hat{G}^+\hat{G}=\hat{I}$. In the general case, $\hat{G}$ may be not unitary, which means $\hat{G}^+\hat{G}=\hat{A}\neq\hat{I}$, where the superscript + indicates the Hermitian conjugation operation, $\hat{I}$ is an identity transform, and $\hat{A}$ is a Hermitian operator.

In numerical simulation, the continuous function must be represented by a set of discrete sampling points. Assume that the number of sampling points along the radial direction on the input plane is N_1. Note N_z is the number of the sampling planes along the optical axis in the output region, N_2 is the number of the sampling points along the radial direction on the output plane, and N_λ is the number of the illumination wavelengths. Equations (1) and (3) can be written in matrices as

$$\mathbf{U}_{1,i\alpha}(r_{1,i},\lambda_\alpha)=\rho_{1,i\alpha}(r_{1,i},\lambda_\alpha)$$
$$\times\exp[i2\pi(n_\alpha-1)h_1(r_{1,i})/\lambda_\alpha], \quad (4)$$

$$\mathbf{U}_{2,j\alpha\beta}(r_{2,j},\lambda_\alpha,z_\beta)=\rho_{2,j\alpha\beta}(r_{2,j},\lambda_\alpha,z_\beta)$$
$$\times\exp\,[i\phi_{2,j\alpha\beta}(r_{2,j},\lambda_\alpha,z_\beta)], \quad (5)$$

$$\mathbf{U}_{2,j\alpha\beta}(r_{2,j},\lambda_\alpha,z_\beta)=\sum_{i=1}^{N_1}\hat{\mathbf{G}}_{ij\alpha\beta}(r_{1,i},r_{2,j},\lambda_\alpha,z_\beta)$$
$$\times\mathbf{U}_{1,i\alpha}(r_{1,i},\lambda_\alpha),$$

where $\hat{\mathbf{G}}_{ij\alpha\beta}(r_{1,i},r_{2,j},\lambda_\alpha,z_\beta)$ corresponds to an $N_1\times N_2\times N_\alpha\times N_z$ matrix and $i=1,2,3,\ldots,N_1$, $j=1,2,3,\ldots,N_2$, $\alpha=1,2,\ldots,N_\lambda$, and $\beta=1,2,3,\ldots,N_z$. Here $h_{1,i}$ represents the surface-relief depth at the i'th sampling point of the DPE. Our aim is to find the surface-relief structure $h_{1,i}(r_{1,i})$ of the DPE that can produce three-color PNDBs characterized by constant and segmented axial-illuminance distributions. In each segment only one color persists. To evaluate the closeness of the calculated wavefront $\hat{G}U_1$ to the expected wavefront U_2, we introduce the following error function D^2.

$$D^2=\sum_{\beta=1}^{N_z}\sum_{\alpha=1}^{N_\lambda}|U_{2,\alpha\beta}-\hat{G}_{\alpha\beta}U_{1,\alpha}|^2$$
$$=\sum_{\beta=1}^{N_z}\sum_{\alpha=1}^{N_\lambda}\mathrm{Tr}\{U_{2,\alpha\beta}^+U_{2,\alpha\beta}-U_{2,\alpha\beta}^+\hat{G}_{\alpha\beta}U_{1,\alpha}$$
$$-U_{1,\alpha}^+\hat{G}_{\alpha\beta}U_{2,\alpha}+U_{1,\alpha}^+A_{\alpha\beta}U_{1,\alpha}\}$$
$$=\left(\frac{1}{N_2}\right)\sum_{\beta=1}^{N_z}\sum_{\alpha=1}^{N_\lambda}\left(\sum_j\rho_{2,j\alpha\beta}^2+\sum_{l,k}\rho_{1,i\alpha}\rho_{1,k\alpha}A_{ikj\alpha\beta}\right.$$
$$\times\exp[-i(\phi_{1,i\alpha}-\phi_{1,k\alpha})]-\sum_{j,k}\{\rho_{2,j\alpha\beta}\rho_{1,k\alpha}G_{kj\alpha\beta}$$
$$\left.\times\exp[-i(\phi_{2,j\alpha\beta}-\phi_{1,k\alpha})]\}+\mathrm{c.c.}\right), \quad (6)$$

where $\hat{A}\equiv\hat{G}^+\hat{G}$ and c.c. represents complex conjugation. We introduce a phase parameter ϕ_0 for a reference wavelength λ_0, $\phi_{1,\alpha}$ can be represented by $\phi_0\lambda_0(n_\alpha-1)/\lambda_\alpha(n_0-1)$, where n_0 is the refractive index at reference wavelength λ_0. The reference wavelength λ_0 and its value are discussed in Sec. 3. Consequently the design problem of the DPE can be formulated as the search for the minimum of D^2 with respect to the arguments $\phi_{0,k}$, i.e., $\partial D^2/\partial\phi_{0,k}=0$. The variation of D^2 with respect to $\phi_{0,k}$ is given by

Downloaded From: http://opticalengineering.spiedigitallibrary.org/ on 04/27/2014 Terms of Use: http://spiedl.org/terms

$$\frac{\partial D^2}{\partial \phi_{0,k}} = \frac{i}{N_2}\sum_{\beta}^{N_z}\sum_{\alpha}^{N_\lambda}\left[\frac{\lambda_0(n_\alpha-1)}{\lambda_\alpha(n_0-1)}\right]\left[\sum_{i}^{N_1}\left\{\rho_{1,i\alpha}\rho_{1,k\alpha}A_{ikj\alpha\beta}\times\exp\left[-i(\phi_{0,i}-\phi_{0,k})\frac{\lambda_0(n_\alpha-1)}{\lambda_\alpha(n_0-1)}\right]-\text{c.c.}\right\}-\sum_{j}^{N_2}\left(\rho_{2,j\alpha\beta}\rho_{1,k\alpha}G_{kj\alpha\beta}\times\exp\left\{-i\left[\phi_{2,j\alpha\beta}-\phi_{0,k}\frac{\lambda_0(n_\alpha-1)}{\lambda_\alpha(n_0-1)}\right]\right\}-\text{c.c.}\right)\right]=0. \tag{7}$$

Then we can assume

$$\mathrm{Im}[Q_k\exp(i\phi_{0,k})]=0, \tag{8}$$

where

$$Q_k=\sum_{\beta}^{N_z}\sum_{\alpha}^{N_\lambda}\left[\left(\sum_{i}^{N_1}\left\{\rho_{1,i\alpha}A_{ikj\alpha\beta}\exp\left[-i\phi_{0,i}\frac{\lambda_0(n_\alpha-1)}{\lambda_\alpha(n_0-1)}\right]\right\}-\sum_{j}^{N_2}[\rho_{2,j\alpha\beta}G_{kj\alpha\beta}\exp(-i\phi_{2,j\alpha\beta})]\right)\times\frac{\lambda_0(n_\alpha-1)}{\lambda_\alpha(n_0-1)}\rho_{1,k\alpha}\exp\left\{i\phi_{0,k}\left[\frac{\lambda_0(n_\alpha-1)}{\lambda_\alpha(n_0-1)}-1\right]\right\}\right]. \tag{9}$$

Finally, the Eq. (8) can be rewritten as

$$\exp[i\phi_{0,k}^{(n,m+1)}]=\frac{\tilde{Q}_k^{*(n,m)}}{|\tilde{Q}_k^{(n,m)}|},\quad k=1,\ldots,N_1, \tag{10}$$

where

$$\tilde{Q}_k^{(n,m)}=\sum_{\beta}^{N_z}\sum_{\alpha}^{N_\lambda}\left[\left(\sum_{i\neq k}^{N_1}\left\{\rho_{1,i\alpha}A_{ikj\alpha\beta}\times\exp\left[-i\phi_{0,i}^{(n,m)}\frac{\lambda_0(n_\alpha-1)}{\lambda_\alpha(n_0-1)}\right]\right\}-\sum_{j}^{N_2}[\rho_{2,j\alpha\beta}G_{kj\alpha\beta}\exp(-i\phi_{2,j\alpha\beta})]\right)\times\frac{\lambda_0(n_\alpha-1)}{\lambda_\alpha(n_0-1)}\rho_{1,k\alpha}\times\exp\left\{i\phi_{0,k}^{(n,m)}\left[\frac{\lambda_0(n_\alpha-1)}{\lambda_\alpha(n_0-1)}-1\right]\right\}\right].$$

Thus we have

$$\exp(i\phi_{2,j\alpha\beta})=\frac{\Sigma_k^{N_1}G_{kj\alpha\beta}\rho_{1,k}\exp\{-i\phi_{0,k}[\lambda_0(n_\alpha-1)/\lambda_\alpha(n_0-1)]\}}{|\Sigma_k^{N_1}G_{kj\alpha\beta}\rho_{1,k}\exp\{-i\phi_{0,k}[\lambda_0(n_\alpha-1)/\lambda_\alpha(n_0-1)]\}|},\quad j=1,2,\ldots,N_2. \tag{11}$$

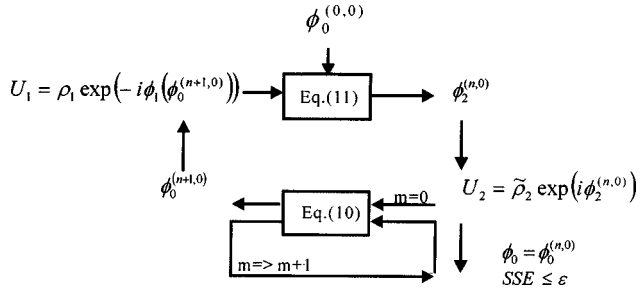

Fig. 2 Flow chart of the iterative algorithm for the phase-retrieval method.

Generally speaking, Eq. (10) cannot be solved analytically, but can be numerically solved by using an iterative algorithm.[19–21] Figure 2 shows the flow chart of the iterative procedures. The iterative procedures are described as following steps. First, we start with a random real value for $\phi_{0,k}$, for example, $\phi_{0,k}^{(0,0)}$. Substituting them and the known amplitude $\rho_{1,k}$ into Eq. (11), we can obtain $\phi_{2,j\alpha\beta}$. Second, substituting $\phi_{0,k}^{(0,0)}$, $\phi_{2,j\alpha\beta}^{(0,1)}$, and the known amplitudes $\rho_{1,k}$ and $\rho_{2,j\alpha\beta}$ into Eq. (10), we can obtain $\phi_{0,k}^{(0,1)}$ and $\rho_{2,j\alpha\beta}^{(0,1)}$. Third, we set $\phi_{0,k}=\phi_{0,k}^{(0,1)}$ and $\phi_{2,j\alpha\beta}=\phi_{2,j\alpha\beta}^{(0,1)}$. To get a quick convergence, in this case we always take the expected amplitude $\tilde{\rho}_{2,j\alpha\beta}$ as $\rho_{2,j\alpha\beta}$. Then substituting them into Eq. (10), we can obtain $\phi_{0,k}^{(0,2)}$. Then $\phi_{0,k}^{(0,2)}$ and $\phi_{2,j\alpha\beta}^{(0,1)}$ are the next estimates of $\phi_{0,k}$ and $\phi_{2,j\alpha\beta}$, respectively. This procedure (step 3) is repeated until the following condition is satisfied:

$$\sum_{k=1}^{N_1}|\phi_{\theta,k}^{(0,m)}-\phi_{0,k}^{(0,m+1)}|\le\varepsilon_1, \tag{12}$$

where ε_1 is a given small value, and m is the number of iterations. At the end of this step we set $\phi_{0,k}^{(1,0)}=\phi_{0,k}^{(0,m+1)}$ and repeat steps 1 to 3 again. The iterative calculation is terminated when the following sum squared error (SSE):

$$\mathrm{SSE}=\frac{\Sigma_{\beta=1}^{N_z}\Sigma_{\alpha=1}^{N_\lambda}\Sigma_{j=1}^{N_2}|\tilde{\rho}_{2,j\alpha\beta}^2-|U_{2,j\alpha\beta}|^2|}{\Sigma_{\beta=1}^{N_z}\Sigma_{\alpha=1}^{N_\lambda}\Sigma_{j=1}^{N_2}|\tilde{\rho}_{2,j\alpha\beta}^2|} \tag{13}$$

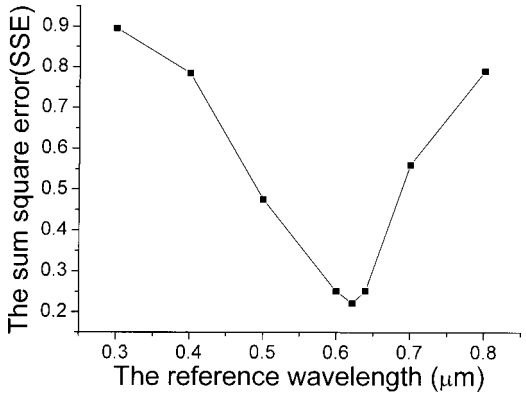

Fig. 3 SSE as the function of the reference wavelength λ_0.

Downloaded From: http://opticalengineering.spiedigitallibrary.org/ on 04/27/2014 Terms of Use: http://spiedl.org/terms

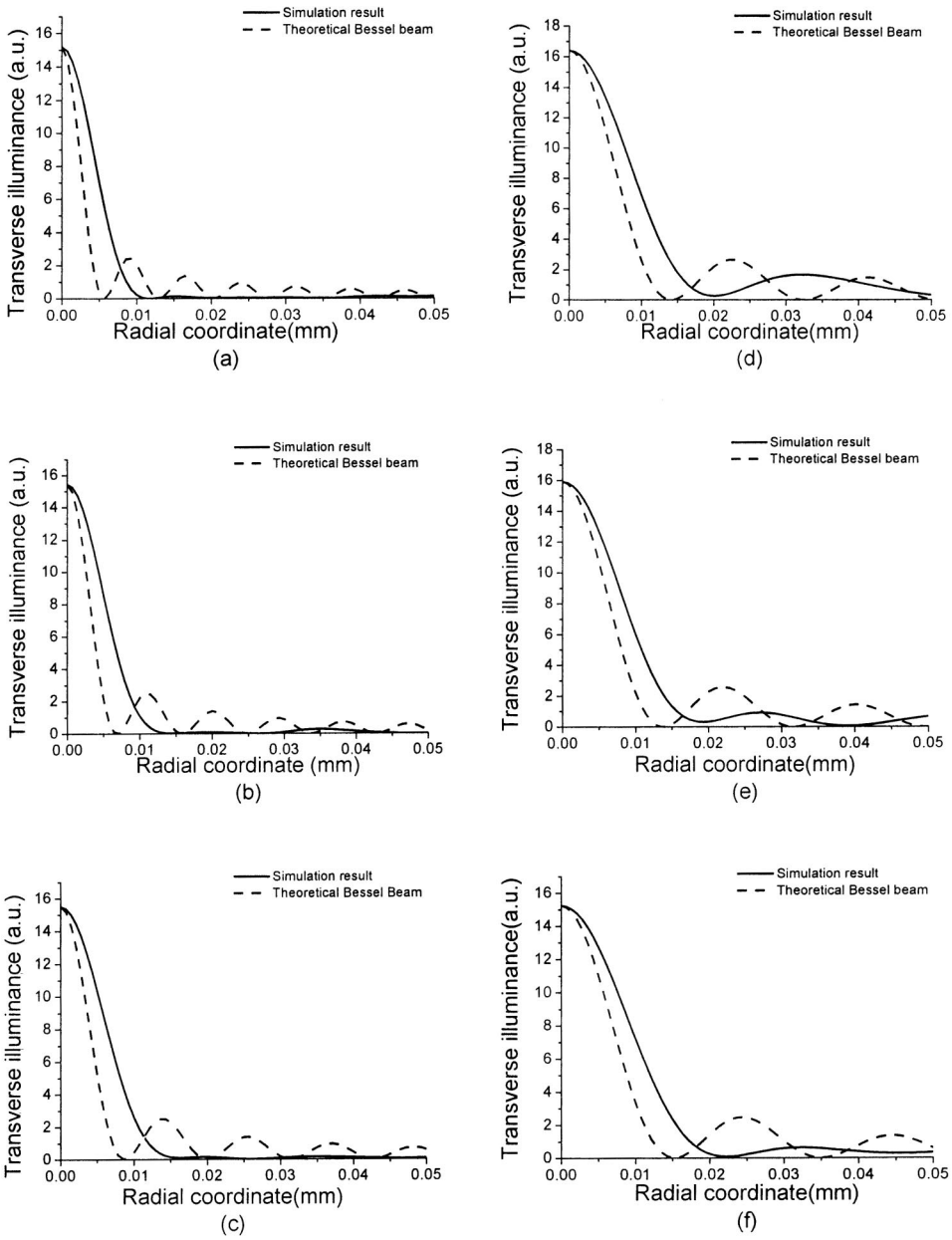

Fig. 4 Comparisons between the transverse illuminance distributions of the simulated PNDB and a Bessel beam on the sampling plane at (a) $z=140$ mm for wavelength 0.6328 μm, (b) $z=210$ mm for wavelength 0.5145 μm, (c) $z=280$ mm for wavelength 0.488 μm, (d) $z=350$ mm for wavelength 0.6328 μm, (e) $z=420$ mm for wavelength 0.5145 μm, and (f) $z=490$ mm for wavelength 0.488 μm. Solid curves represent the transverse illuminance distributions of the PNDB generated by the DPE on the sampling planes, and dashed curve represent the illuminance distributions of the zero-order Bessel beam of the first kind.

reachs minimum, which determines the calculation accuracy. Finally, the surface-relief profile $h_{1,k}$, given by Eq. (14), for the DPE can be determined by

$$h_{1,k}=\frac{\lambda_0\phi_{0,k}}{2\pi(n_0-1)}, \quad k=1,2,\ldots,N_1. \tag{14}$$

3 Simulation and Experimental Result

The desired PNDB contains six segments along the optical axis with constant axial illuminance distribution and is monochromatic in each segment. The first and fourth segments for $\lambda_1=0.6328$ μm correspond to the regions [120 mm, 170 mm] and [330 mm, 380 mm], respectively; the second and fifth segments for $\lambda_2=0.5145$ μm correspond to the regions [190 mm, 240 mm] and [400 mm, 450 mm], respectively; the third and sixth segments for $\lambda_3=0.488$ μm correspond to the regions [260 mm, 310 mm] and [470 mm, 520 mm], respectively. The parameters used in this design are as follows. The diameter of the DPE and the incident plane-wave beam are $2R_{1m}=6.0$ mm. The

Downloaded From: http://opticalengineering.spiedigitallibrary.org/ on 04/27/2014 Terms of Use: http://spiedl.org/terms

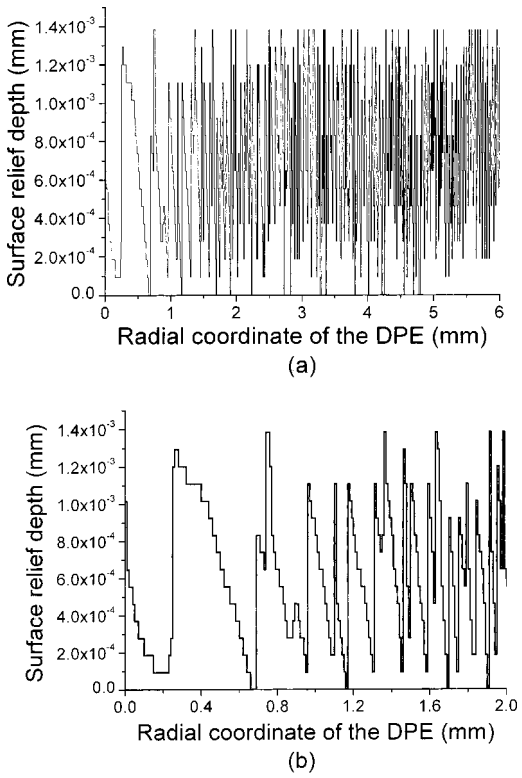

Fig. 5 Distribution of the surface-relief depth of the designed 16-level DPE (a) for full and (b) for part.

numbers of sampling points on the input and output planes are $N_1=600$ and $N_2=20$, respectively. For the calculation of the axial illuminance distribution, the interval Δz between the sampling planes must satisfy the sampling condition[9] that is given by

$$\Delta z \leqslant 2\pi \frac{z^2}{kR_{1m}^2 - 2\pi z}, \tag{15}$$

where $k=2\pi/\lambda$ is the wave number of the incident light. Thus the maximum sampling interval that can be determined by Eq. (15) is 0.1357 mm. According to the theoretical expressions, the number of the sampling points along the optical axis in the output space is $N_z=3420$, and the sampling interval is $\Delta z=0.1316$ mm in our design. The number of wavelengths for the illumination light is $N_\lambda=3$. We assume that the incident wave for each color is plane wave so the illuminance on the DPE is considered to be uniform. In this calculation we find that the reference wavelength λ_0 could affect the final by reached SSE. The results for different λ_0 values are shown in Fig. 3. We can see that we have the best result if the reference wavelength λ_0 is 0.631 μm. The output amplitude distribution $\tilde{\rho}_{2,j\alpha\beta}$ is given to be the expected value.

The transverse illuminance distributions of the beam generated by the designed DPE on the each sampling plane are shown in Figs. 4(a) to 4(f), where the solid curves represent the transverse illuminance distributions of the beam generated by the DPE on the sampling planes, and the dashed curves represent the illuminance distributions of the zero-order Bessel beam of the first kind. We clearly see that the multisegment beam has a transverse illuminance distribution near a Bessel beam distribution. The deviations indicate that the DPE is not real nondiffracting.

To meet the requirement of our fabrication process, the obtained optimum continuous surface profile must be quantized in the multilevel structure. Figure 5 shows the surface-relief structures of the DPE in 16 levels. The simulation of axial-illuminance distributions with higher sampling points generated by the designed 16-level DPE is shown in Fig. 6. From our simulation, we find that N_1, N_z, and λ_0 play important roles in the optimization. There are some restrictions on the two parameters N_1 and N_z. For instance, the minimum feature size permitted for the fabrication process determines the upper limit of N_1. When the values of N_1 and N_z increase, the computation becomes more complicated. To ensure convergence for the algorithm, we relax the restriction of initial condition. In the beginning calculation, we start with a smaller number of sampling points along the optical axis $N_z=180$. Then, we use more sampling points and substitute the result that is calculated before as initial phase ϕ_0 in the next calculation process. Finally, the number of the sampling points N_z is increased to 3420 in the last calculation.

The fabrication process of the DPE is as follows. First, four photographic masks (shown in Fig. 7) were generated by a laser beam pattern generator (Model HIMT DWL 2.0). Then optical contact lithography and reactive-ion etching (Model AB 1500-series) were used to fabricate the surface-relief structures of the DPE on a flat quartz substrate. The minimum feature size of the fabricated element is 10 μm. Figure 8 shows a photograph of the fabricated DPE and Table 1 shows the etching-depth errors in the etching process. Figure 9 shows the part of the profile for the surface-relief structure of the fabricated DPE scanned with a Sloan Dektak profilemeter. To check the performance of the fabricated DPE, we measured the illuminance distributions on the sampling planes around the optical axis. The experimental setup for this measurement is shown in Fig. 10. The illumination beam consists of a He-Ne laser (0.6328 μm) and a multiline Argon laser (0.5145 μm, 0.488 μm). A CCD camera was placed on the optical bench and moved along the optical axis to record the output images on serial sampling planes. The measured axial illuminance distribution is shown in Fig. 11. We also measured the transverse illuminance distributions around the optical axis. The measured results are shown in Figs. 12(a) to 12(f), measured for λ_1, λ_2 and λ_3 at $z=140$ mm located in the first segment, at $z=210$ mm located in the second segment, at $z=280$ mm located in the third segment, at $z=350$ mm located in the fourth segment, at $z=420$ mm located in the fifth segment, and at $z=490$ mm located in the sixth segment, respectively. These results clearly indicate that the fabricated DPE can produce the desired six-segment three-color PNDBs.

To appraise the performance of the designed DPE, we must calculate the diffraction efficiency and SNR. The diffraction efficiency for each wavelength on the sampling plane is defined as

$$\eta(\lambda_\alpha)=\frac{\phi_{\text{signal}}(\lambda_\alpha)}{\phi_{\text{input}}(\lambda_\alpha)}, \quad \alpha=1,2,3, \tag{16}$$

Downloaded From: http://opticalengineering.spiedigitallibrary.org/ on 04/27/2014 Terms of Use: http://spiedl.org/terms

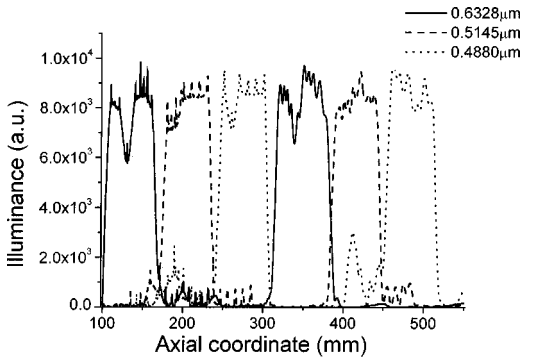

Fig. 6 Axial-illuminance distribution of the three-color PNDB with six segments.

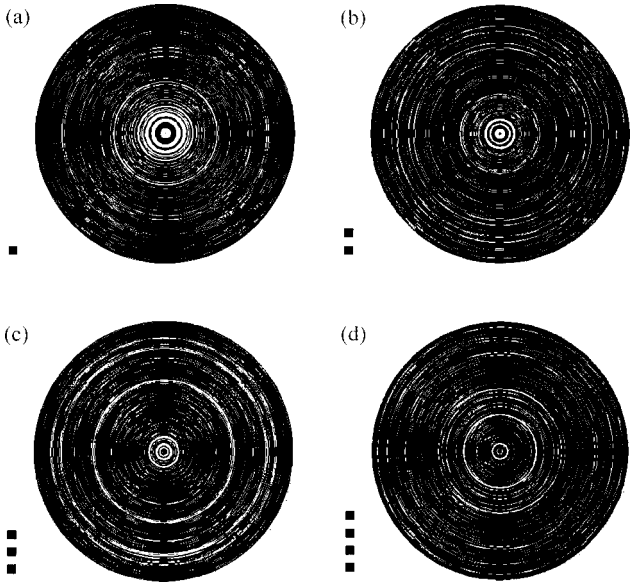

Fig. 7 Photographic masks for 16-level DPE: (a) mask 1, (b) mask 2, (c) mask 3, and (d) mask 4.

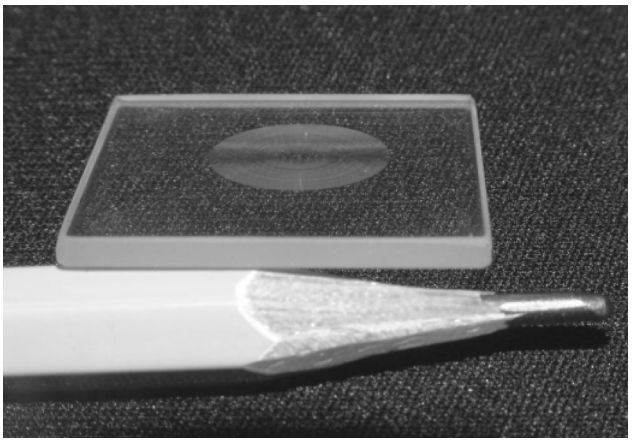

Fig. 8 Photograph of the fabricated sample.

Table 1 Etching-depth errors in the etching process by using reactive-ion etching (RIE).

	Theoretical Etching Depth (μm)	Measured Etching Depth (μm)	Error Ratio (%)
Mask 1	0.738468	0.7599	2.9
Mask 2	0.369234	0.3717	0.6
Mask 3	0.184617	0.1933	0.8
Mask 4	0.092308	0.0953	3.2

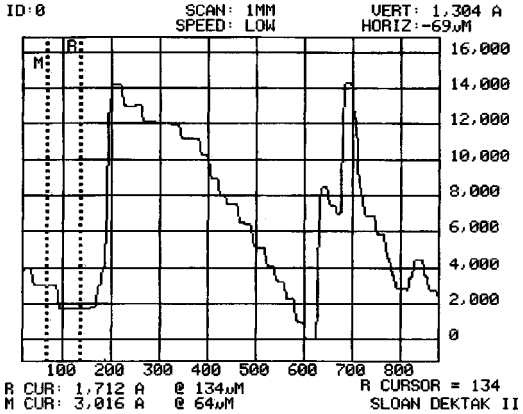

Fig. 9 Section profile of the surface-relief trace of the 16-level DPE obtained by scanning with a Sloan Dektak profilemeter.

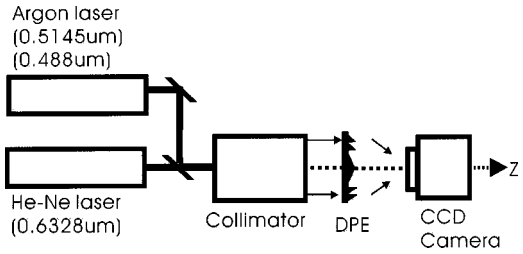

Fig. 10 Experimental setup for measuring the characteristics of the designed 16-level DPE.

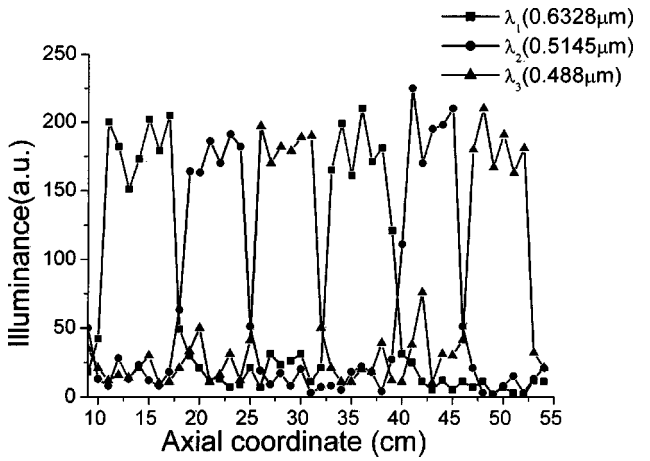

Fig. 11 Measured axial-illuminance distribution generated by the 16-level DPE.

Downloaded From: http://opticalengineering.spiedigitallibrary.org/ on 04/27/2014 Terms of Use: http://spiedl.org/terms

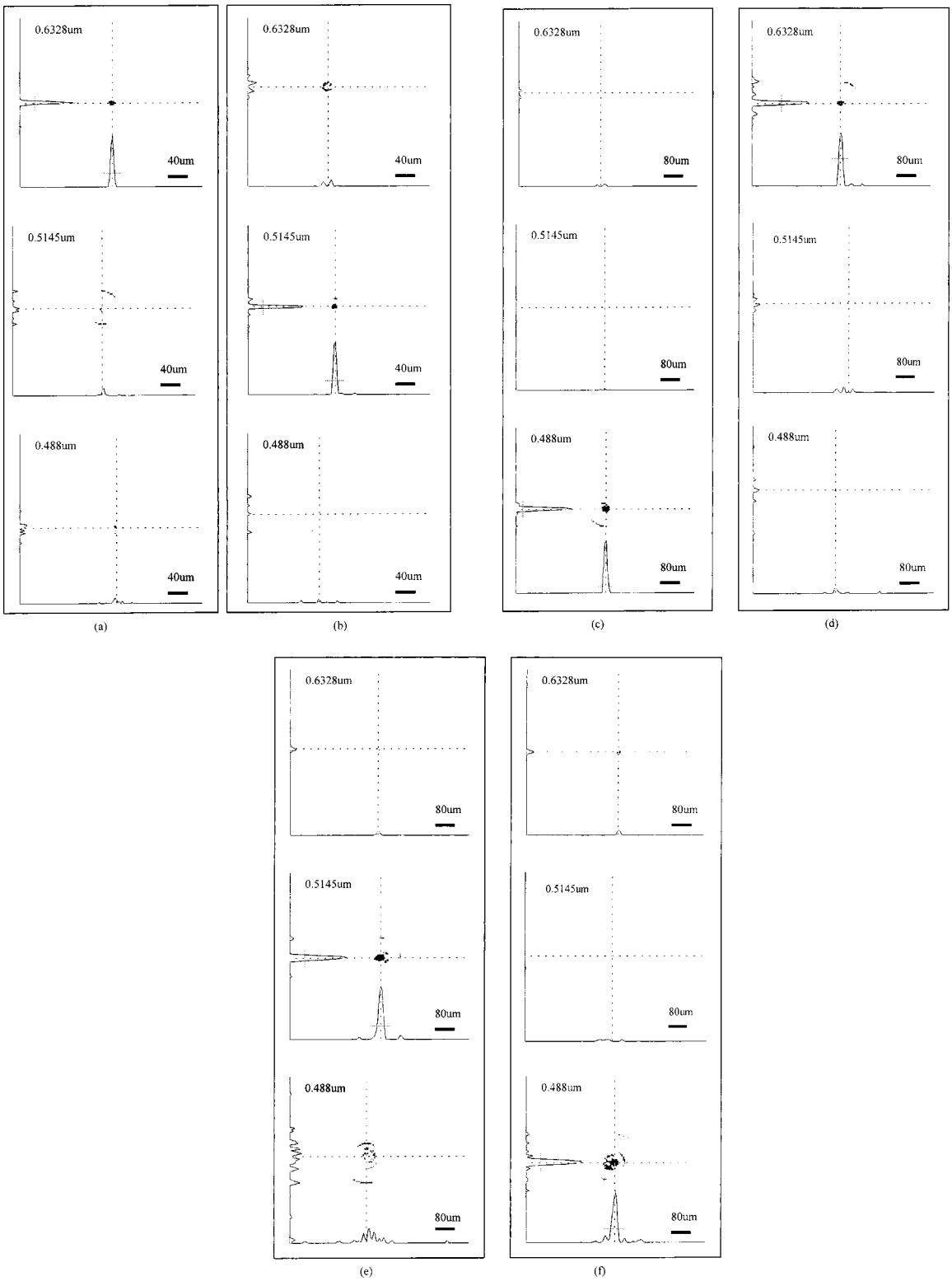

Fig. 12 Transverse illuminance distributions for three wavelengths on the sampling plane at (a) $z = 140$ mm, (b) $z = 210$ mm, (c) $z = 280$ mm, (d) $z = 350$ mm, (e) $z = 420$ mm, and (f) $z = 490$ mm.

Downloaded From: http://opticalengineering.spiedigitallibrary.org/ on 04/27/2014 Terms of Use: http://spiedl.org/terms

Table 2 Theoretical and measured diffraction efficiencies and SNRs for each wavelength.

Distance between Input Plane and Output Plane (sample plane) (mm)	Signal Wavelength (μm)	Efficiency (%)		SNR	
		Theoretical	Measured	Theoretical	Measured
140	0.6328	33.2	26.7	8.6	4.2
210	0.5145	32.1	25.1	8.9	3.8
280	0.488	32.5	24.6	9.3	3.2
350	0.6328	38.4	23.2	23.1	3.5
420	0.5145	34.5	25.8	4.1	2.2
490	0.488	30.9	19.4	15.8	5.1

where $\phi_{\text{input}}(\lambda_\alpha)$ is the total incident flux at λ_α on the input plane, and $\phi_{\text{signal}}(\lambda_\alpha)$ is the total flux over the signal region on the sampling plane for λ_α.

The SNR represents the ratio of the signal flux of the wavelength focused in the segment to the flux of the other wavelengths on the same area, and can be expressed as

$$\text{SNR}(\lambda_\alpha)=\frac{\Sigma_{\text{signal}} I(r_{2,\text{signal}},\lambda_\alpha)}{\Sigma_{\alpha'\neq\alpha}\Sigma_{\text{noise}} I(r_{2\,\text{noise}},\lambda_{\alpha'})}, \quad \alpha=1,2,3. \qquad (17)$$

Table 2 represents the diffraction efficiency and SNR for each wavelength.

4 Summary

We described the design of a three-color PNDBs in a multiple chromatic illuminating system and showed the results of simulation for the designed DPE. In Fig. 4, the simulations show that the transverse illuminance distribution of the PNDB is near to that of a Bessel beam.

The designed 16-level structure DPE has been fabricated on a flat quartz substrate by optical contact lithography and RIE. Experiments show that 6-segment PNDBs can be well formed in the preset regions when a collimated laser beam is used to illuminate the fabricated DPE. The experimental results are in good agreement with the numerical simulations, which verifies the design method. Owing to the novel features of the three-color PNDBs, it is expected that the proposed DPE can be useful in applications of precision alignment, display, and optical interconnection in multiple chromatic illuminating systems.

Acknowledgments

The authors gratefully acknowledge the National Science Council of the Republic of China for financial support of this research under Project No. NSC 89-2215-E-009-084, and the Semiconductor Research Center of the National Chiao-Tung University where the DPE was fabricated.

References

1. J. N. Mait, ''Understanding diffractive optic design in the scalar domain,'' *J. Opt. Soc. Am. A* **12**, 2145–2158 (1995).
2. R. Piestun and J. Shamir, ''Control of wave-front propagation with diffractive elements,'' *Opt. Lett.* **19**, 771–773 (1994).
3. V. V. Kotiyar, S. N. Khonina, and V. A. Soifer, ''Algorithm for the generation of non-diffracting Bessel modes,'' *J. Mod. Opt.* **43**, 1231–1239 (1995).
4. C. Paterson and R. Smith, ''Higher-order Bessel waves produced by axicon-type computer-generated holograms,'' *Opt. Commun.* **124**, 121–130 (1996).
5. C. Paterson and R. Smith, ''Helicon waves: propagation-invariant waves in a rotating coordinate system,'' *Opt. Commun.* **124**, 131–140 (1996).
6. L. Niggl, T. Lanzl, and M. Maier, ''Properties of Bessel beams generated by periodic gratings of circular symmetry,'' *J. Opt. Soc. Am. A* **14**, 27–33 (1997).
7. B.-Z. Dong, G.-Z. Yang, B.-Y. Gu, and O. K. Erosy, ''Iterative optimization approach for designing an axicon with long focal depth and high transverse resolution,'' *J. Opt. Soc. Am. A* **13**, 97–103 (1996).
8. B. Salik, J. Rosen, and A. Yariv, ''One-dimensional bean shaping,'' *J. Opt. Soc. Am. A* **12**, 1702–1706 (1995).
9. R. Piestun, B. Spektor, and J. Shamir, ''Wave fields in three dimensions: analysis and synthesis,'' *J. Opt. Soc. Am. A* **13**, 1837–1848 (1996).
10. R. Piestun, B. Spektor, and J. Shamir, ''Unconventional light distribution in three-dimensional domains,'' *J. Mod. Opt.* **43**, 1495–1507 (1996).
11. V. V. Kotlyar, S. N. Khonina, and V. A. Soifer, ''Iterative calculation of diffractive optical elements focusing into a three-dimensional domain and onto the surface of the body of rotation,'' *J. Mod. Opt.* **43**, 1509–1524 (1996).
12. R. Lieu, B.-Y. Gu, B.-Z. Dong, and G.-Z. Yang, ''Design of diffractive phase elements that realize axial-intensity modulation based on the conjugate-gradient method,'' *J. Opt. Soc. Am. A* **15**(3), 689–694 (1998).
13. J. Durnin, J. J. Miceli, Jr., and J. H. Eberly, ''Diffractive-free beams,'' *Phys. Rev. Lett.* **58**, 1499–1501 (1987).
14. V. P. Koronkevitch and I. G. Palchikova, ''Kinoforms with increased depth of focus,'' *Optik (Jena)* **87**, 91–93 (1991).
15. J. R. Fienup, ''Gradient-search phase retrieval algorithm: for inverse synthetic aperture radar,'' *Opt. Eng.* **13**, 3237–3242 (1994).
16. J. Rosen, B. Salik, and A. Yariv, ''Pseudo-nondiffracting beams generated by radial harmonic functions,'' *J. Opt. Soc. Am. A* **12**, 2446–2457 (1995).
17. R. Liu, B.-Z. Dong, G.-Z. Yang, and B.-Y. Gu, ''Generation of pseudo-nondiffracting beams with use of diffractive phase elements designed by the conjugate-gradient method,'' *J. Opt. Soc. Am. A* **15**(1), 144–151 (1998).
18. R. Liu, B.-Z. Dong, G.-Z. Yang, and B.-Y. Gu, ''Implementation of pseudo-nondiffracting beams by use of diffractive phase elements,'' *Appl. Opt.* **37**(35), 8219–8223 (1998).
19. R. Liu, B.-Y. Gu, B.-Z. Dong, and G.-Z. Yang, ''Diffractive phase elements that synthesize color pseudo-nondiffracting beams,'' *Opt. Lett.* **23**, 633–635 (1998).
20. G. Yang, B. Gu, X. Tan, M. P. Chang, B. Dong, and O. K. Ersoy, ''Iterative optimization approach for the design of diffractive phase elements simultaneously implementing several optical functions,'' *J. Opt. Soc. Am. A* **11**, 1632–1640 (1994).
21. G. Yang, B. Gu, and B. Dong, ''Theory of the amplitude-phase retrieval in any linear transform system and its applications,'' *Int. J. Mod. Phys. B* **7**, 3153–3224 (1993).
22. G. Z. Yang, B. Z. Dong, B. Y. Gu, J. Y. Zhuang, and O. K. Ersoy, ''Gerchberg-Saxton and Yang-Gu algorithms for phase retrieval in a nonunitary transform system: a comparison,'' *Appl. Opt.* **33**, 209–218 (1994).

Downloaded From: http://opticalengineering.spiedigitallibrary.org/ on 04/27/2014 Terms of Use: http://spiedl.org/terms

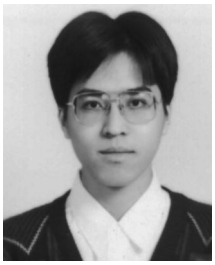

Jyh-Rou Sze received his BS degree in 1997 from the Department of Electrical-Engineering, Private Chinese-Culture University, and his MS degree in 1999 from the Department of Electro-Optical Engineering, Nation Chiao-Tung University, where he is currently working toward his PhD degree. His current interests include numerical methods applied to design diffractive optical elements that have a particular function and to fabricate the designed elements.

Mao-Hong Lu graduated from the Department of Physics, Fudan University, in 1962. He was then a research staff member with the Shanghai Institute of Physics and Technology, Chinese Academy of Sciences, from 1962 to 1970, and with the Shanghai Institute of Laser Technology from 1970 to 1980. He studied at the University of Arizona as a visiting scholar from 1980 to 1982. He is currently a professor with the Institute of Electro-optical Engineering, Nation Chiao-Tung University.

Downloaded From: http://opticalengineering.spiedigitallibrary.org/ on 04/27/2014 Terms of Use: http://spiedl.org/terms